



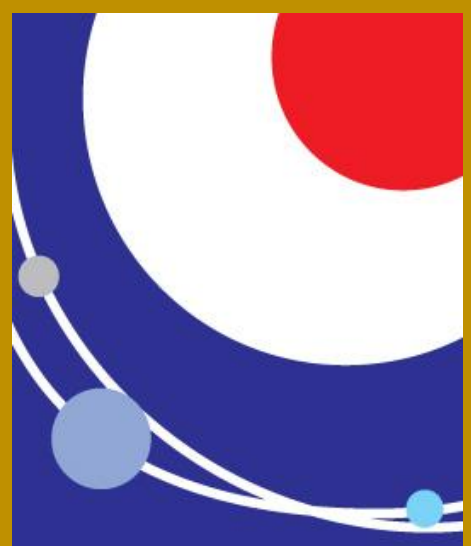
University
of Colorado
Boulder

Statistical Analysis of Impulsiveness and Rise Phase Duration of Solar Flares in the He II 304 Angstrom Chromospheric Line

Cole A Tamburri (1); Maria D Kazachenko (1, 2, 3); Adam F Kowalski (1, 2, 3)

(1) Department of Astrophysical and Planetary Sciences, University of Colorado, Boulder; (2) National Solar Observatory;

(3) Laboratory for Atmospheric and Space Sciences



1. Introduction: Flare Impulsiveness Index

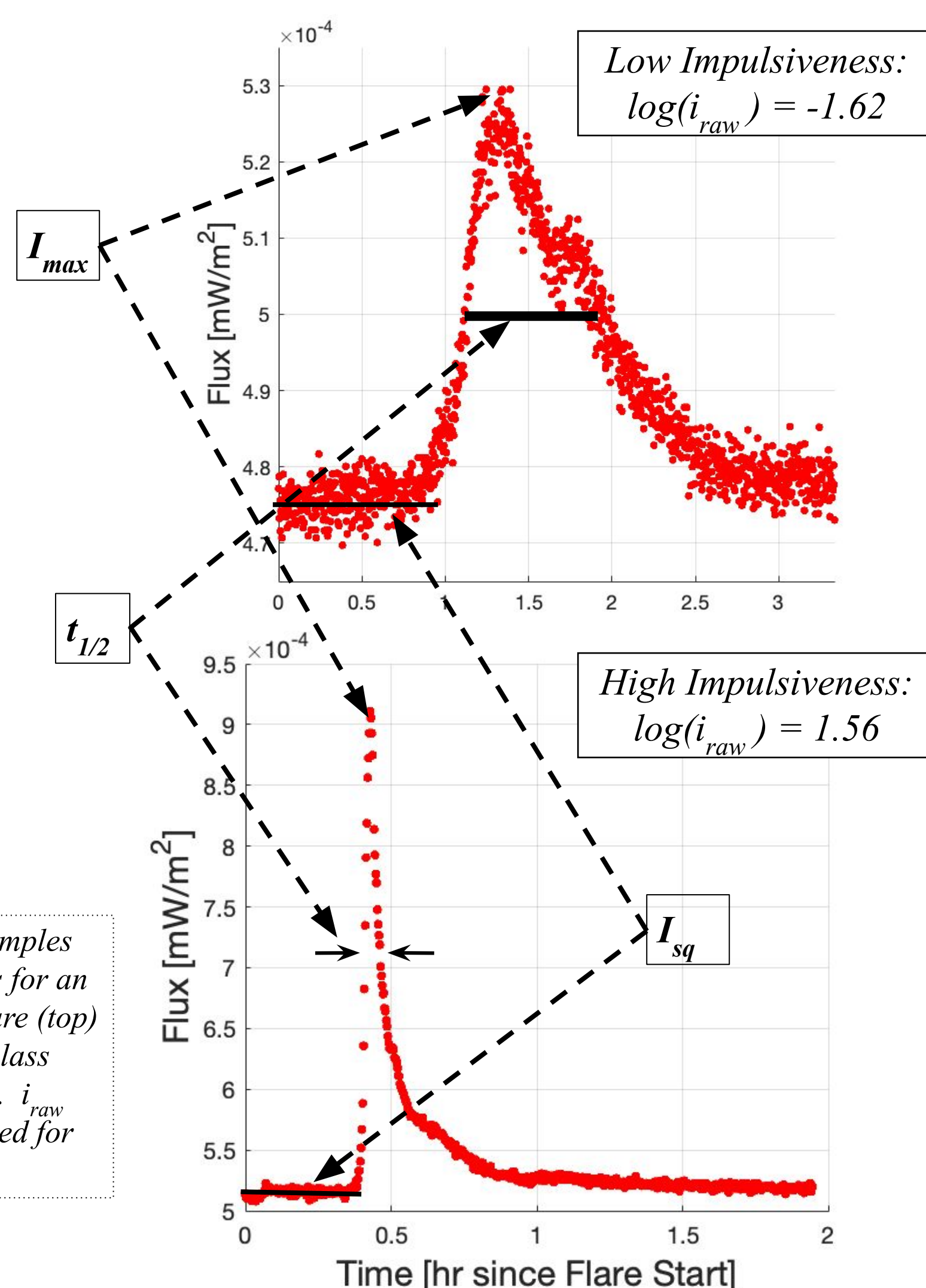
Abstract:

Why are some solar and stellar flares impulsive while others are not? We develop a classification system for solar flares based on the impulsiveness index presented for stellar flares by Kowalski et al. (2013). We use the RibbonDB database (Kazachenko et al. 2017) to study 2048 flares from 2010 - 2014, and SDO/EVE 304 Å data to develop the impulsiveness index. We use full-disk SDO/AIA 1600 Å images to study morphological variations and develop an algorithm to identify key flare parameters. For a selection of 500 flares, we compare the impulsiveness index to other quantities associated with solar flares. Finally, we use a semi-autonomous method to identify polarity inversion lines (PILs) and analyze parallel and perpendicular ribbon motion for a selection of flares in the context of impulsiveness.

$$i_{raw}(t) = \frac{I_{max}}{t_{1/2}}$$

$$i_{scaled}(t) = \frac{I_{max} - I_{sq}}{I_{sq} t_{1/2}}$$

Figure 1: Examples of light curves for an M1.0-class flare (top) and an X1.8-class flare (bottom). i_{raw} values are listed for both flares.



3. Results: Statistics; Impulsiveness Index vs. Flare Properties

Distribution of Flare Impulsiveness

We divide the flares into bins of impulsiveness. A broken power law is the best model for the impulsiveness bins of the population.

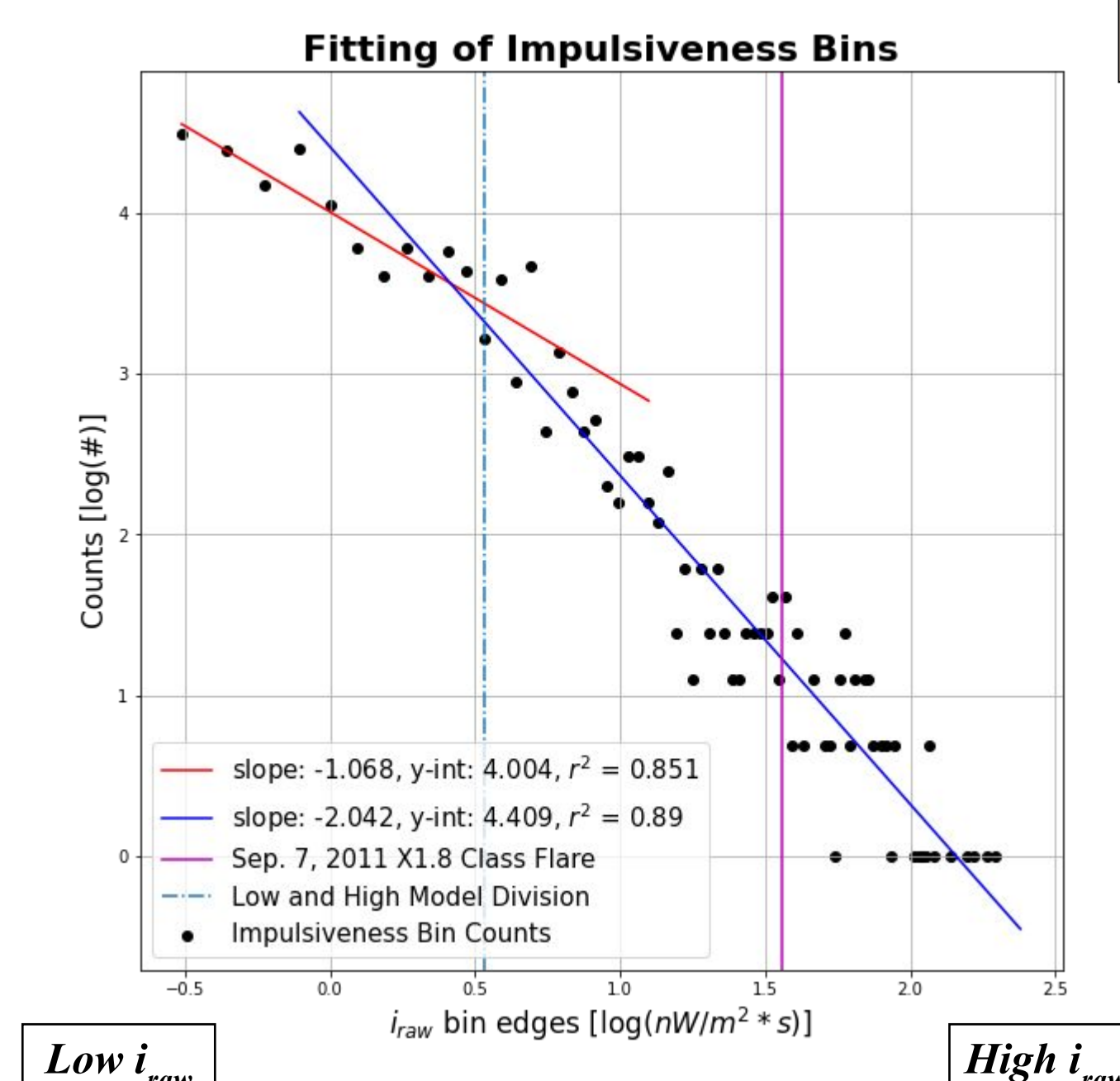


Figure 4: Fitting of the impulsiveness bin counts for all flares in the sample, with low impulsiveness bins removed to account for the detection limit. The high impulsiveness flare (Fig. 1, bottom) is indicated by the magenta line; the low impulsiveness flare (Fig. 1, top) and flares listed in panel 4 are beyond the lower limit of the bins shown.

QPP Period

Hayes et al. (2020) present a statistical study of **stationary QPP periods** for flares in the RibbonDB database and compare to a number of other flare quantities. The relationship between QPP period and impulsiveness follows the dependence between impulsiveness and duration.

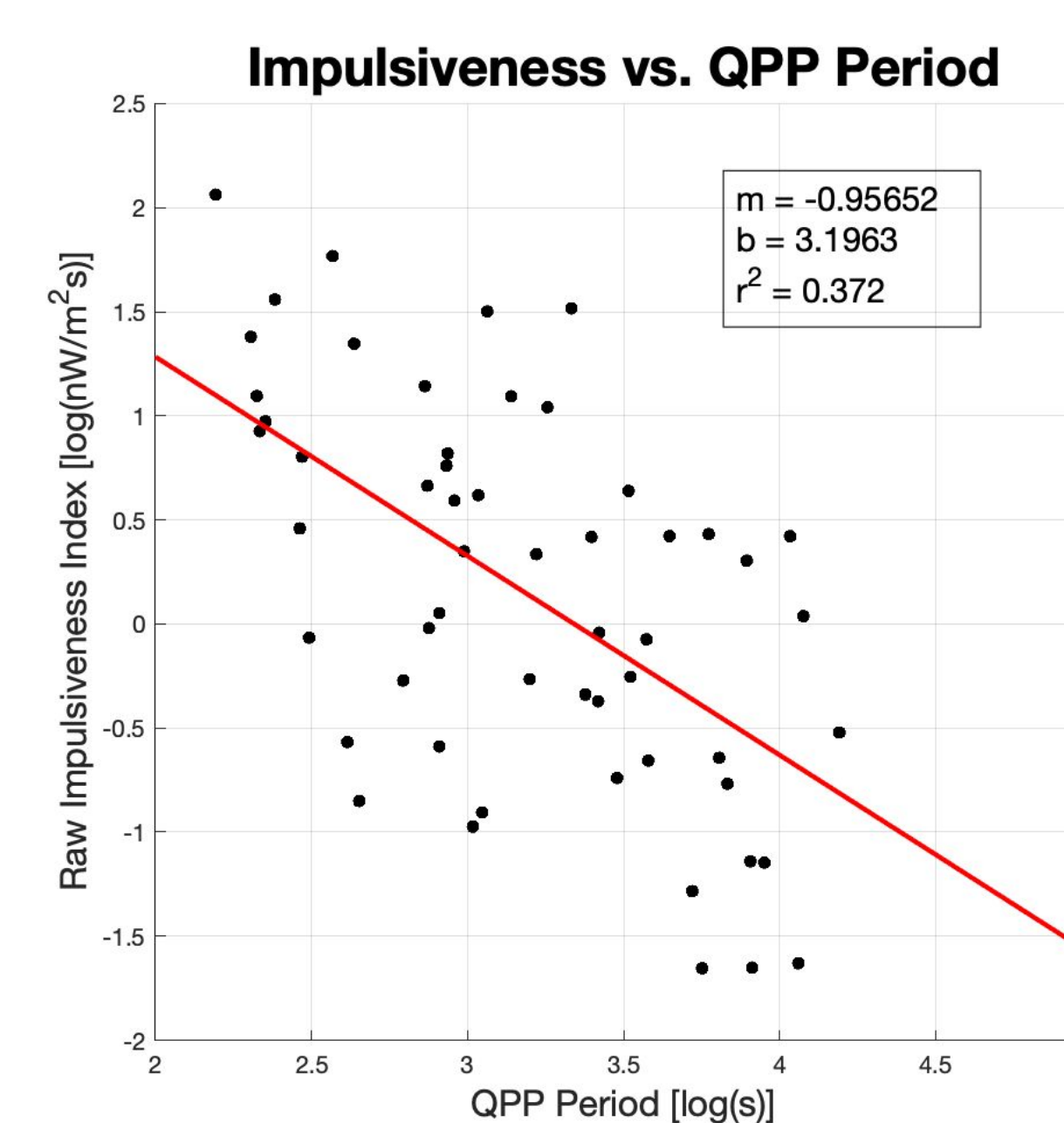


Figure 5: Impulsiveness vs. QPP Period for the 500 best-performing flares which have stationary QPP signatures as identified by Hayes et al. (2020).

Flare Duration

The relationship between impulsiveness and **flare duration** resembles a power law fit. Both the rise and decay phase durations (which are not correlated) also show this relationship.

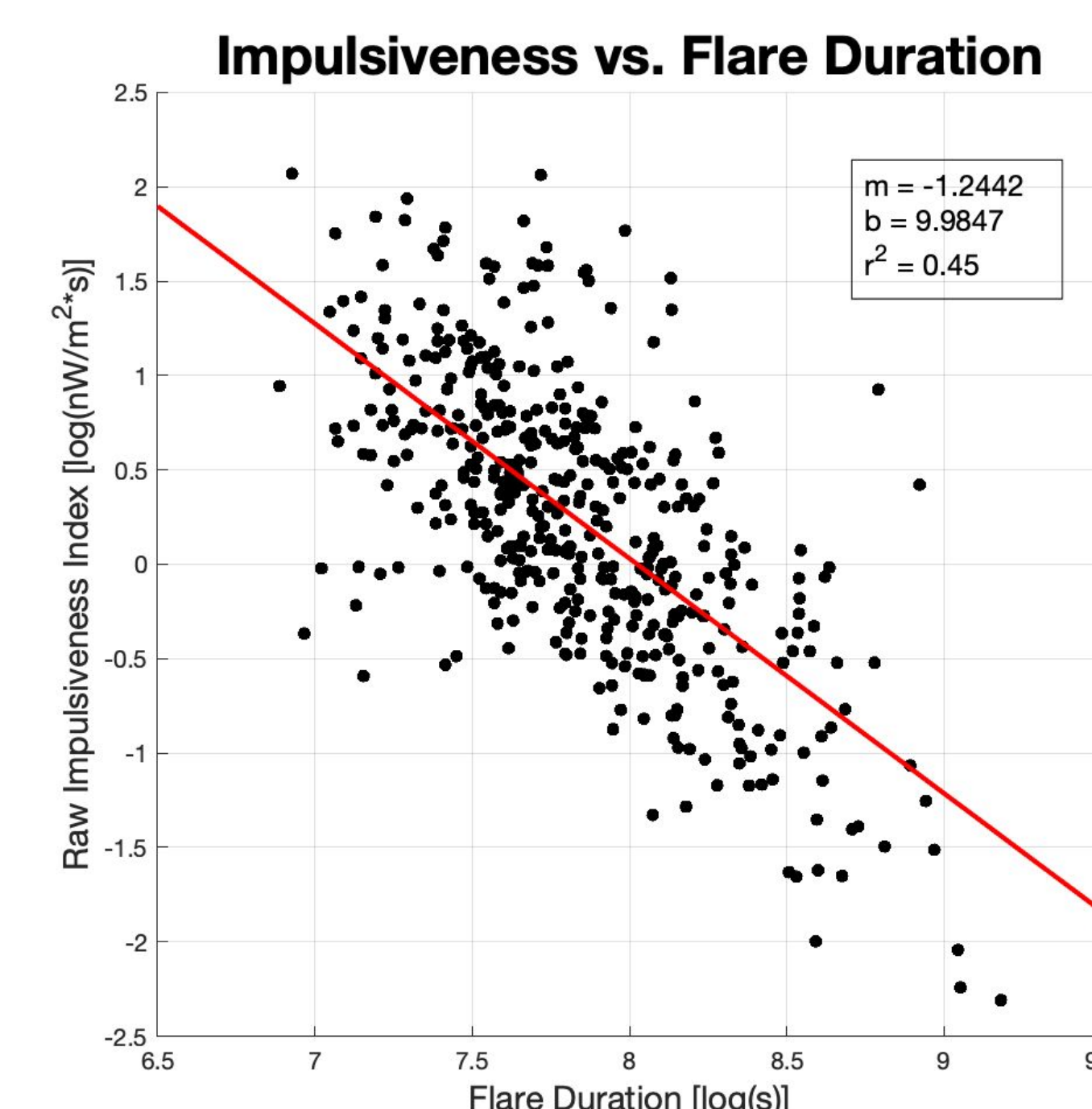


Figure 6: Relationship between impulsiveness and flare duration for the 500 flares referenced in Fig. 4 - in log-log space. "m" is the slope of the best fit line, and "b" is the y-intercept.

Reconnection Rate

The relationship between impulsiveness and **reconnection rate** (maximum reconnection rate in the positive polarity region during the impulsive phase) is weak.

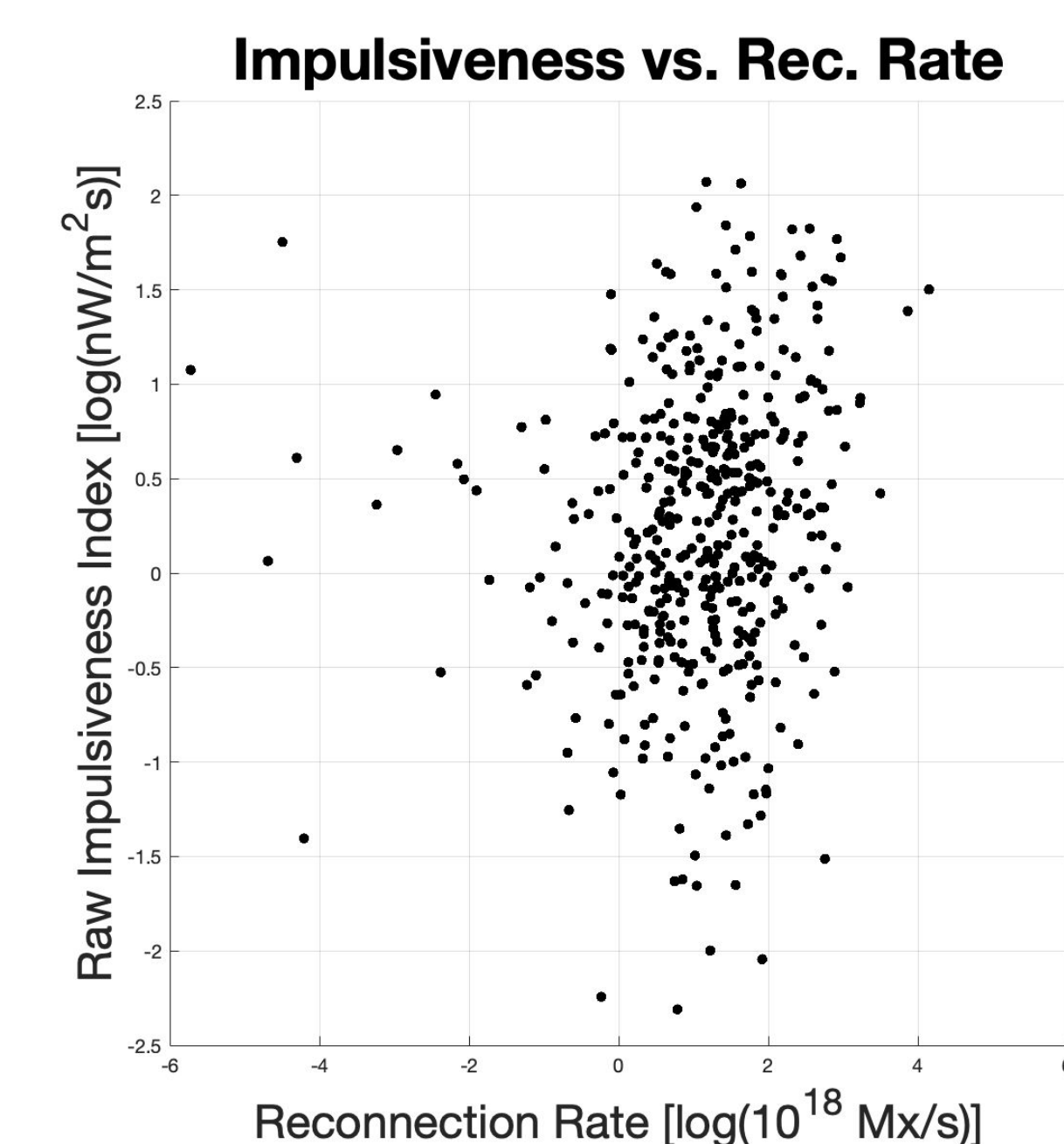


Figure 7: Impulsiveness and maximum reconnection rate in the impulsive phase for the 500 flares referenced in Fig. 4.

2. Methods: Polarity Inversion Line Identification

Next, the parallel and perpendicular motion of the two ribbons relative to the PIL are determined using SDO/AIA 1600 Å masks. This analysis is done for a selection of flares. Particular attention is paid to three flares originating from the same active region (AR11865), allowing for comparison of eruptions resulting from similar magnetic structure.

Using the 1600 Å full-disk images from SDO/AIA, we look more closely at the morphology of ribbons associated with flares. The PIL is determined via a semi-autonomous Gaussian convolution of opposite-polarity HMI masks similar to that presented by Wang et al. (2019), and the 1600 Å images are used to track the parallel and perpendicular motion of the ribbons.

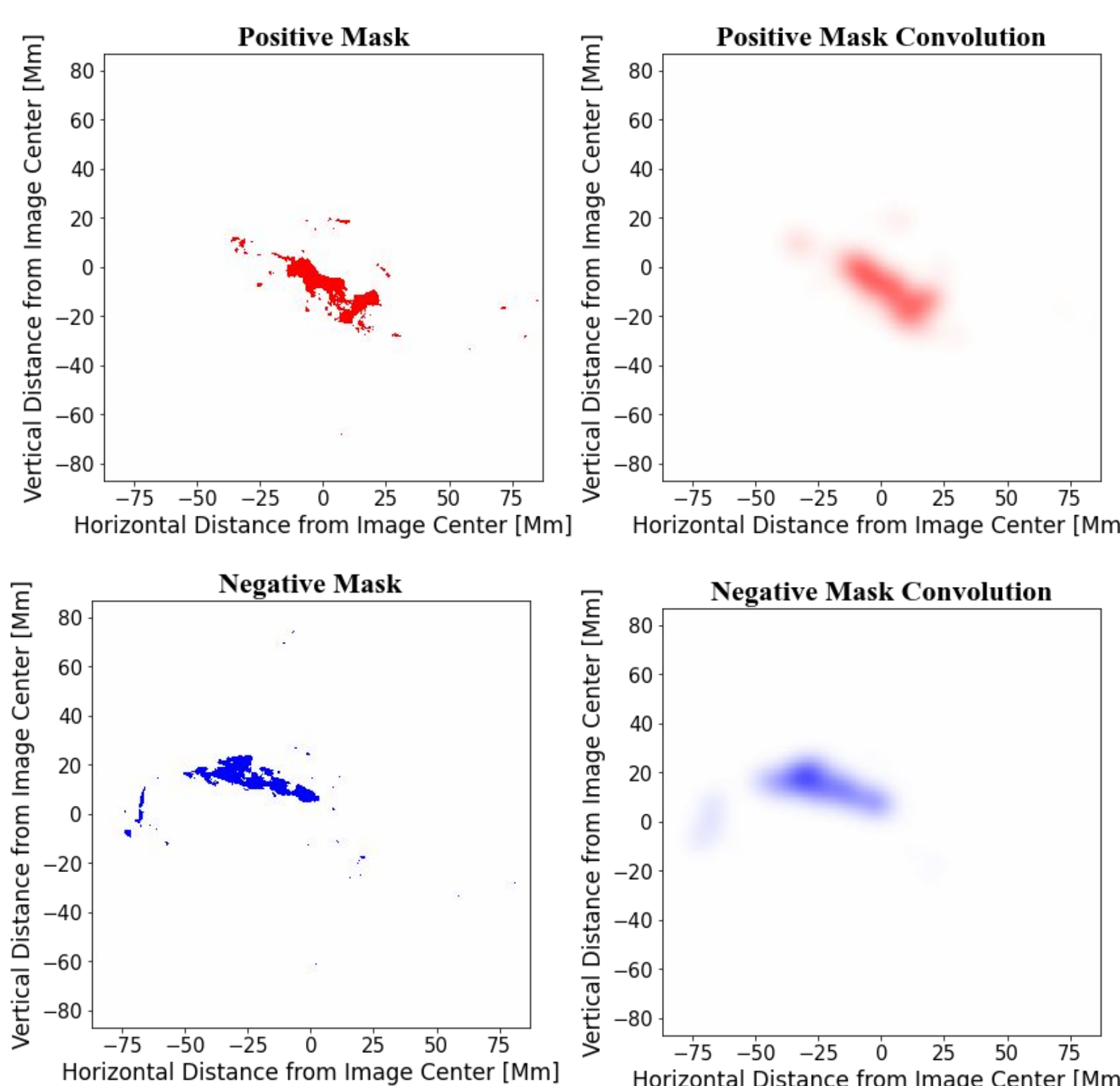


Figure 2: (Left) Sample identification of positive and negative polarity ribbons using SDO/AIA 1600 Å images and HMI magnetograms. (Right) Convolution of ribbon masks with a Gaussian function for use in PIL identification.

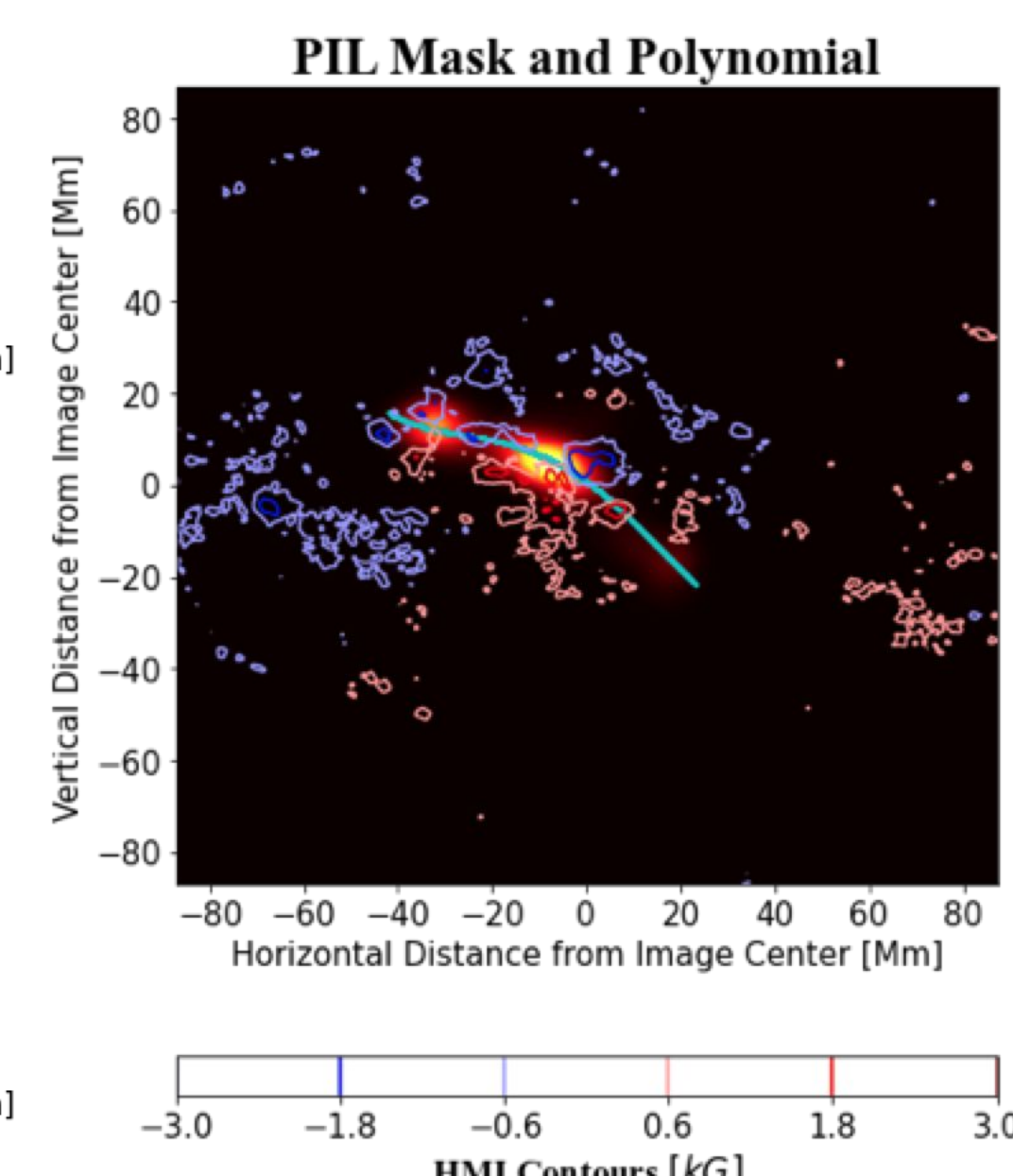


Figure 3: The PIL mask (colormap), polynomial-fitted PIL (cyan line), and HMI magnetic field (contours).

4. Results: Impulsiveness Index vs. Parallel and Perpendicular Ribbon Motion

2013-10-13, AR11865, M1.7 Class Flare [$\log(i_{raw}) = -0.97$]

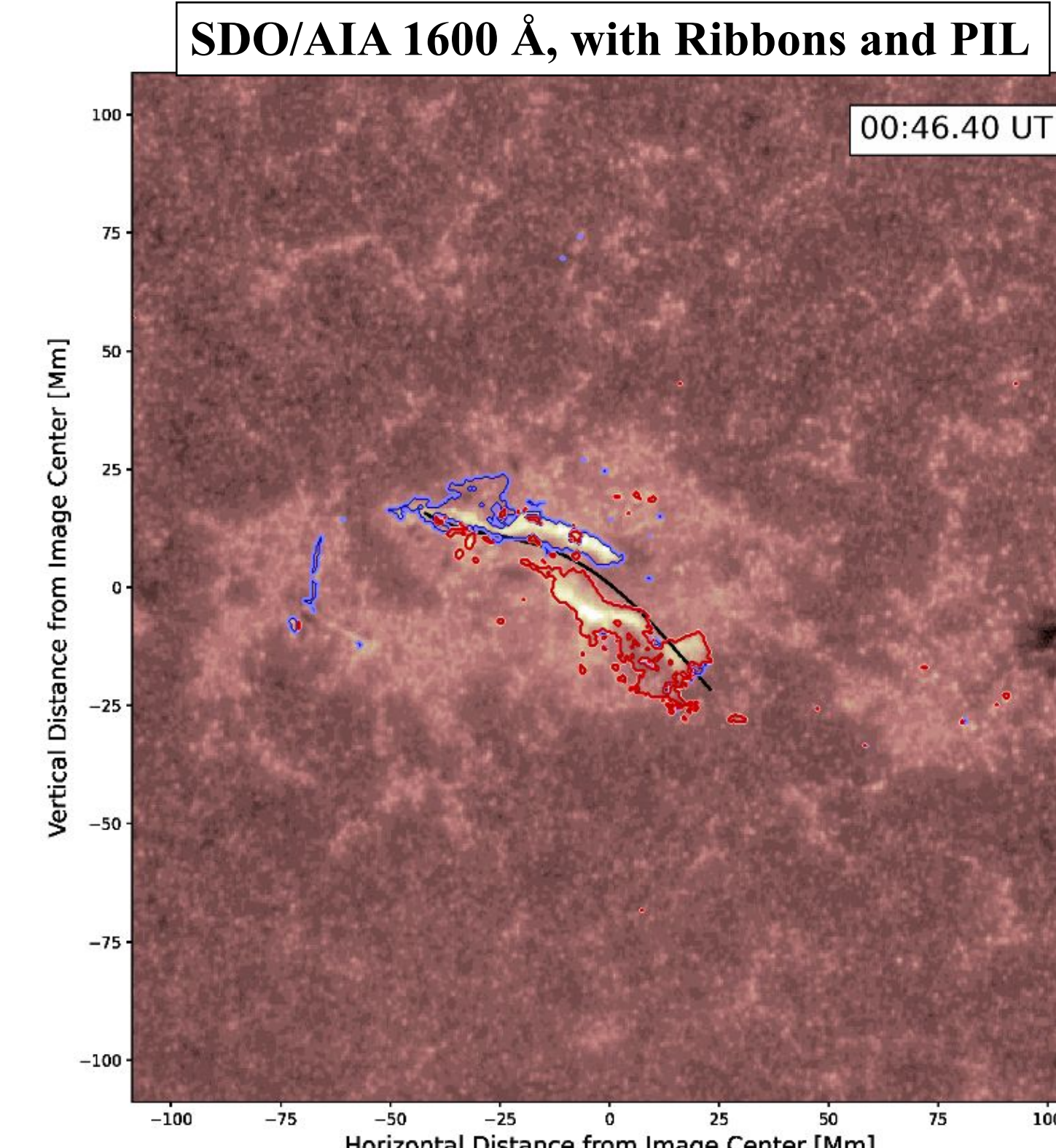
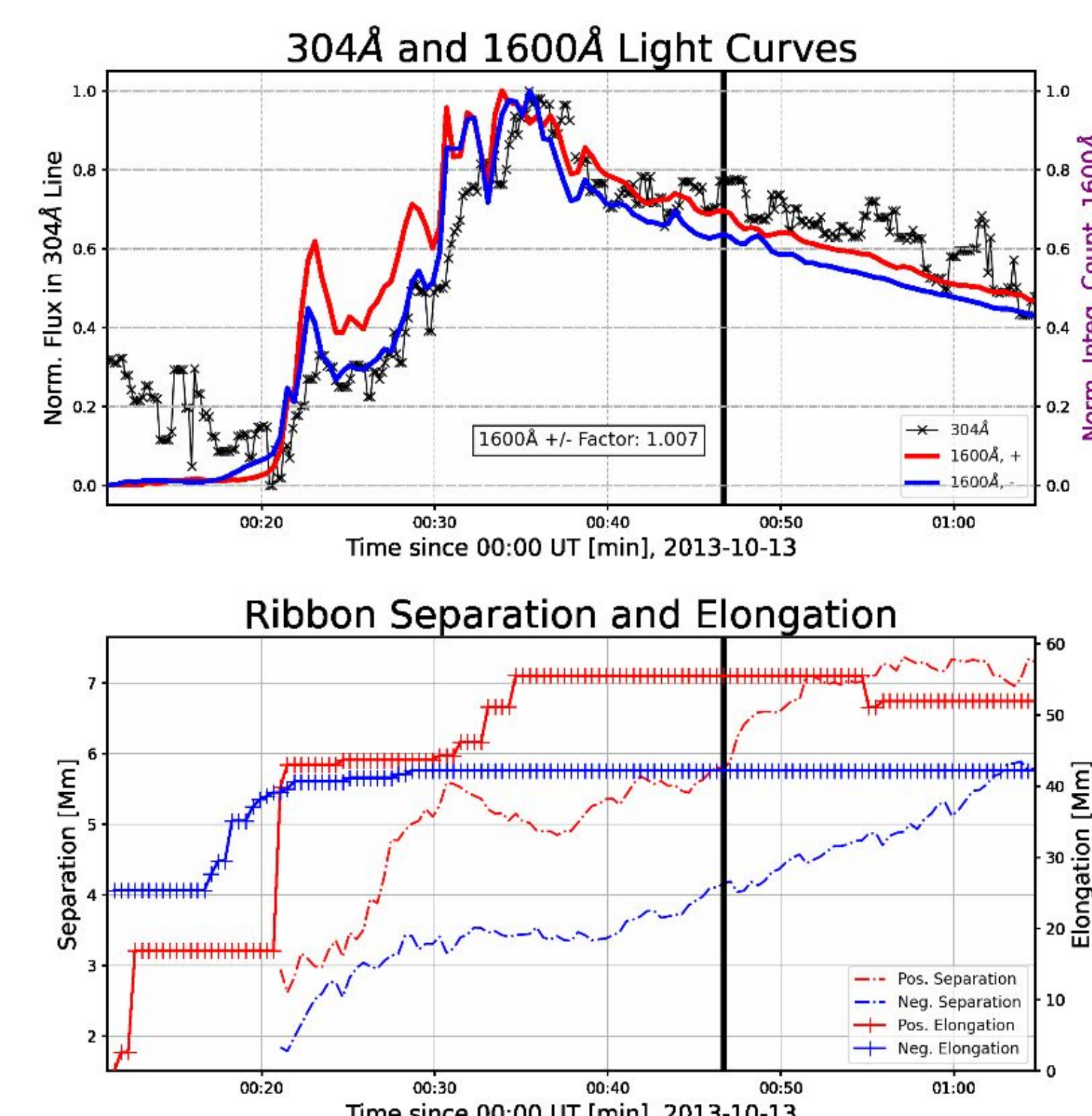


Figure 8: October 13th, 2013 M1.7 class flare in AR11865. Full animation at link below.

Scan the code below for access to visualization of a larger selection of flares, including two others from this active region



Characteristics of Ribbon Morphology:

- Parallel motion tends to dominate rise phase
- Perpendicular motion tends to dominate decay phase
- Evidence for similar impulsiveness in flares of common AR
- Positive and negative ribbon fluxes show similar structure, though some asymmetries exist
- Positive and negative ribbon peak fluxes are not necessarily identical
- Varying degree of magnetic shear
- Elongation motion can be either parallel or antiparallel

Events Included:

- December 26, 2011, Class C5.7, $\log(i_{raw}) = -1.26$
- October 13, 2013, Class M1.7, $\log(i_{raw}) = -0.97$
- October 14, 2013, Class C8.0
- October 15, 2013, Class M1.8, $\log(i_{raw}) = -1.00$
- November 9, 2014, Class M2.3

5. Conclusions and Future Work

- Flare impulsiveness in the 304 Å chromospheric line is related to QPP period and flare duration, but not magnetic reconnection rate.
- There is evidence to suggest that the impulsiveness indices of flares originating from the same active region may be similar.
- Parallel (elongation) and perpendicular (separation) motion of flare ribbons typically correspond to the rise and decay phases of flare development, respectively.
- Positive and negative ribbon light curves are related in structure, though with some important differences, particularly in the time of local and absolute peak fluxes.

Future work: Expansion of the sample of full-disk images, complemented by analysis of associated magnetic field structure, will allow for comparison of the impulsiveness index to magnetic shear and may suggest a relationship with particle acceleration (Dahlin et al. 2021). Application of this work will provide new insight into development of stellar flares.

6. Acknowledgements

C. A. T. thanks the providers of the George Ellery Hale Fellowship in the CU Boulder APS department, as well as the members of the Kazachenko Research Group at CU Boulder. M. D. K. thanks the NASA/HSR grant 80NSSC18K1283. All authors acknowledge and appreciate the support of NSO and LASP.

Works Cited:

- Dahlin, J. T. et al. (2021). Variability of the reconnection guide field in solar flares. *ApJ*, in production.
- Hayes, L. A. et al. (2020). Statistical Study of Goes X-ray quasi-periodic pulsations in solar flares. *ApJ*, 895(1), 50.
- Kazachenko, M. D. et al. (2017). A database of flare ribbon properties from the Solar Dynamics Observatory. I. Reconnection Flux. *ApJ*, 845(1), 49.
- Kowalski, A. F. et al. (2013). Time-resolved properties and global trends in DME flares from simultaneous photometry and Spectra. *ApJ Supplement Series*, 207(1), 15.
- Qiu, J. et al. (2017). Elongation of flare ribbons. *The Astrophysical Journal*, 838(1), 17.
- Wang, J. et al. (2019). Parameters derived from the SDO/HMI vector magnetic field data: Potential to improve machine-learning-based Solar Flare Prediction models. *ApJ*, 884(2), 175.